

# Mechanics and refractive power optimization of tunable acoustic gradient lenses

Euan McLeod<sup>a)</sup> and Craig B. Arnold

*Department of Mechanical and Aerospace Engineering, Princeton University, Princeton, New Jersey 08544*

(Received 13 February 2007; accepted 12 June 2007; published online 8 August 2007)

Tunable acoustic gradient index (TAG) lenses create tunable multiscale Bessel beams. These lenses are fluid-filled cylindrical cavities within which an acoustic radial standing wave is excited. This standing wave modulates the density, and thereby the refractive index within the lens. Spatial gradients in the refractive index can be used for lensing. A predictive model for the steady-state fluid mechanics behind TAG lenses driven with a sinusoidal voltage signal is presented here. The model covers inviscid and viscous regimes in both the resonant and off-resonant cases. The density fluctuations from the fluidic model are related to refractive index fluctuations. The entire model is then analyzed to determine the optimal values of lens design parameters for greatest lens refractive power. These design parameters include lens length, radius, static refractive index, fluid viscosity, sound speed, and driving frequency and amplitude. It is found that long lenses filled with a fluid of high refractive index and driven with large amplitude signals form the most effective lenses. When dealing with resonant driving conditions, low driving frequencies, smaller lens radii, and fluids with larger sound speeds are optimal. At nonresonant driving conditions, the opposite is true: High driving frequencies, larger radius lenses, and fluids with low sound speeds are beneficial. The ease of tunability of the TAG lens through modifying the driving signal is discussed, as are limitations of the model including cavitation and nonlinearities within the lens. © 2007 American Institute of Physics. [DOI: 10.1063/1.2763947]

## I. INTRODUCTION

Since their creation twenty years ago by Durnin,<sup>1</sup> Bessel beams have been extensively studied. Much of this interest is due to the beams' ability to resist diffraction and to heal themselves behind obstructions. As a result, Bessel beams can travel long distances while maintaining small central spot diameters.

Conventionally, Bessel beams have been generated using annular slits,<sup>2,3</sup> refractive axicons,<sup>4,5</sup> and diffractive methods.<sup>6</sup> More recently however, the demand has grown for tunable Bessel beams. Being able to adjust spot size, working distance, and lateral pattern extent without moving parts allows researchers to more rapidly switch the types of patterns they can generate and the size scales of the materials they study.

Bessel beams have been applied to uneven surface texturing,<sup>7</sup> drilling,<sup>8</sup> and bulk transparent material modifications,<sup>9,10</sup> however, the use of *tunable* Bessel beams has not been explored in these areas. In the field of optical manipulation, the demand for tunable Bessel beams has been met with spatial light modulators (SLMs).<sup>11–14</sup> SLMs have provided dynamic optical manipulation at both the microscopic scale,<sup>15–17</sup> and the atomic scale<sup>13,18</sup> by using digital liquid-crystal plates where each pixel can be programmed to introduce a specific phase delay. However, spatial light modulators have some restrictions including their pixellation, low refresh rates (generally video rates around 30 Hz), and low damage thresholds. For example, in optical microman-

ipulation, faster refresh rates would be useful. Changes in trap position on the millisecond time scale have been used to study the statistical mechanics of nonequilibrium processes,<sup>19</sup> and thermal motion on the same time scales has been observed.<sup>20</sup> In atom optics, due to smaller particle sizes, refresh rates greater than 1 kHz are desirable.<sup>21</sup>

In a recent article, we presented an alternative method for creating tunable Bessel beams: The tunable acoustic gradient index of refraction (TAG) lens.<sup>22</sup> Currently, this method does not provide the same resolution or degree of optical control as an SLM; however, TAG lenses do have the advantage of being free of pixellation due to their analog nature, being capable of faster response times limited only by the speed of sound within the lens material,<sup>23</sup> and possessing higher damage thresholds because they are not restricted to using delicate liquid crystals.

A TAG lens uses acoustic waves to modulate the density of an optically transparent fluid, thereby producing a spatially and temporally varying index of refraction—effectively a time-varying gradient index lens. Because the TAG lens operates at frequencies in the order of  $10^5$  Hz, the patterns observed (Fig. 1) by passing a CW collimated laser beam through the TAG lens are time-average images of a temporally periodic pattern. The minor rings around each bright major ring approximate nondiffracting axicon-generated Bessel beams.<sup>22</sup> This article will explain the mechanics behind these patterns.

The TAG lens is a cylindrical cavity formed by a hollow piezoelectric tube with two flat glass windows on either side for optical access, see Fig. 2. The cavity is then filled with a refractive fluid and the piezoelectric is driven with an AC

<sup>a)</sup>Electronic mail: emcleod@princeton.edu

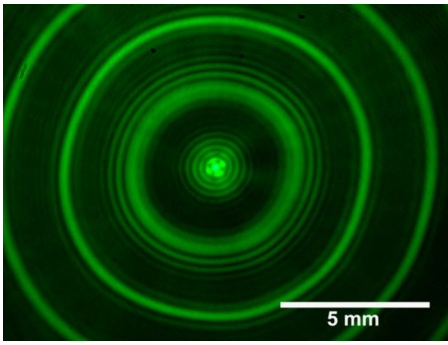


FIG. 1. (Color online) Characteristic pattern created by illuminating a circular TAG lens with a wide Gaussian collimated laser beam. This image is observed 80 cm after the lens, using the base case TAG lens parameters except with the driving frequency shifted to 299.7 kHz.

signal generating vibration in several directions, the most significant being the radial direction. This establishes standing-wave density and refractive index oscillations within the fluid, which are used to shape an incident laser beam.

This article presents a predictive model for the fluid mechanics and local refractive index throughout the lens under steady-state operation. A previous model for an acoustically-driven lens had been proposed,<sup>24</sup> however this model had invoked time-invariant nonlinear acoustic theories which ignore the more significant linear effects occurring in these lenses. Experimentation has shown that TAG beams are strongly time-varying, and the following linear acoustic model better explains all characteristics of the TAG lens. In this article, the results of the model will be provided using the “base case” TAG lens parameters published earlier.<sup>22</sup> Optimizing the refractive capabilities of the lens relative to this base case is also discussed. The effects of modifying the lens dimensions, filling fluid, and driving signal are all examined, as well as how modifying the driving signal can be used to tune the index of refraction within the lens.

## II. BASE CASE PARAMETERS

Because of the large number of parameters involved in designing a TAG lens, we start by assuming experimental parameters similar to those of an existing TAG lens.<sup>22</sup> Those parameters are selected here as the “base case,” to which potential modifications will be compared. Figure 1 shows the

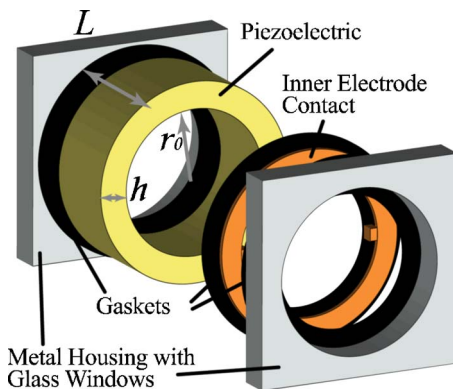


FIG. 2. (Color online) Expanded view of a circular TAG lens.

TABLE I. Base case parameters for the TAG lens, divided into geometric, fluid, and driving signal parameters, respectively.

| Parameter                | Symbol   | Base case value       |
|--------------------------|----------|-----------------------|
| Lens inner radius        | $r_0$    | 3.5 cm                |
| Lens length              | $L$      | 4.06 cm               |
| Fluid viscosity          | $\nu$    | 100 cS                |
| Static refractive index  | $n_0$    | 1.4030                |
| Speed of sound           | $c_s$    | 1.00 km/s             |
| Fluid density            | $\rho_0$ | 964 kg/m <sup>3</sup> |
| Voltage amplitude        | $V_A$    | 10 V                  |
| Peak inner wall velocity | $v_A$    | 1 cm/s                |
| Resonant frequency       | $f$      | 246.397 kHz           |
| Off-resonant frequency   | $f$      | 253.5 kHz             |

pattern generated by a base case TAG lens (except for a shifted driving frequency) as observed 80 cm behind the lens. The lens itself is diagrammed in Fig. 2. The base case parameters for this lens are listed in Table I.

The piezoelectric material used is lead zirconate titanate, PZT-8, and the filling fluid for the lens is a Dow Corning 200 Fluid, a silicone oil. The piezoelectric is driven by a function generator (Stanford Research Systems, DS345) passed through an RF amplifier (T&C Power Conversion, AG 1006) and impedance matching circuit, which can produce ac voltages up to 300  $V_{pp}$  at frequencies between 100 kHz and 500 kHz. Other impedance matching circuits could be used to facilitate different frequency ranges. Two different driving frequencies are used, corresponding to resonant and off-resonant cases, listed in Table I.

## III. MECHANICS

### A. Piezoelectric transduction

The piezoelectric transducer used to drive the TAG lens comes in the form of a hollow cylinder. The electrodes are placed on the inner and outer circumferences of the cylinder. We assume that we can set the driving voltage frequency and amplitude applied to the piezoelectric so that

$$V = V_A \sin(\omega t). \quad (1)$$

The theory behind how a hollow tube piezoelectric will respond to such a driving voltage has already been published.<sup>25</sup> Their work will not be reproduced here, however, this theory leads to inner wall velocities on the order of  $v_A = 1$  cm/s, assuming driving voltage amplitudes on the order of 10 V. It is important to note that the wall velocity is always proportional to the driving voltage amplitude.

### B. Fluid mechanics

The mechanics of the fluid within the lens is described by three equations: Conservation of mass, conservation of momentum, and an acoustic equation of state. Stated symbolically, these equations are

$$\frac{\partial \rho}{\partial t} + \nabla \cdot (\rho \mathbf{v}) = 0, \quad (2)$$

$$\frac{\partial}{\partial t}(\rho \mathbf{v}) + \nabla p + \nabla \cdot (\rho \mathbf{v} \otimes \mathbf{v}) + \nabla \cdot \mathbf{D} = 0, \quad (3)$$

$$p - p_0 = c_s^2(\rho - \rho_0), \quad (4)$$

where  $\otimes$  represents the tensor product and  $\mathbf{D}$  is the viscous stress tensor whose elements are given by

$$D_{ij} = -(\eta - 2\mu/3)(\nabla \cdot \mathbf{v})\delta_{ij} - \mu\left(\frac{\partial v_i}{\partial x_j} + \frac{\partial v_j}{\partial x_i}\right). \quad (5)$$

Here,  $\rho$  is the local density,  $\mathbf{v}$  is the local fluid velocity,  $p$  is the local pressure,  $\mu$  is the dynamic shear viscosity, and  $\eta$  is the dynamic bulk viscosity. Bulk viscosities are not generally tabulated and are difficult to measure. For most fluids,  $\eta$  is the same order of magnitude as  $\mu$ .<sup>26–28</sup> For the base case, we have assumed that  $\eta = \mu$ . Equation (4) assumes small amplitude waves where  $c_s$  is the speed of sound within the fluid at the quiescent density and pressure,  $\rho_0$  and  $p_0$ . This equation represents the linearized form of all fluid equations of state.

Substituting the equation of state [Eq. (4)] into the momentum conservation equation [Eq. (3)] yields two coupled differential equations for the dependent variables  $\rho$  and  $\mathbf{v}$ . Applying no-slip conditions at the boundaries of the cell translates to these boundary conditions

$$\mathbf{v}|_{r=r_0} = v_A \cos(\omega t) \hat{\mathbf{r}}, \quad (6)$$

$$\mathbf{v}|_{z=0} = \mathbf{v}|_{z=L} = 0. \quad (7)$$

The radial boundary condition is determined from the velocity of the inner wall of the piezoelectric. This assumes that the piezoelectric is stiff compared to the fluid and that acoustic waves within the fluid do not couple back into the piezoelectric motion. Impedance spectroscopy conducted on the TAG lens shows that except near resonances, the TAG lens impedance is the same regardless of the filling fluid chosen. Hence, this assumption is generally true, however, some corrections may be needed when near resonance. The presence of the gaskets (see Fig. 2) will also modify the boundary condition in Eq. (6), however, this effect is neglected in this article, because it is expected to only be significant near the gaskets themselves.

Typically, a unique solution for  $\rho$  and  $\mathbf{v}$  at all times would require two initial conditions as well as the above boundary conditions. However, for the purposes of this paper, we are only concerned with the steady-state response to the vibrating wall, and the initial conditions do not affect the steady-state response.

The following assumptions reduce the dimensionality of the problem, making it more tractable. First, the azimuthal dependence can be eliminated because of the lack of angular dependence within the boundary conditions [Eqs. (6) and (7)]. Second, the  $z$  dependence of the boundary conditions only appears in the no-slip conditions at the glass windows. Physically, this effect is expected to be localized to a boundary layer of approximate thickness<sup>29</sup>

$$\delta = \sqrt{\frac{2\mu}{\rho_0\omega}}. \quad (8)$$

For the base case parameters, this thickness comes out to approximately 10  $\mu\text{m}$ . Thus, the lens is operating in the limit  $\delta \ll L$ , and solving the problem outside the boundary layer will account for virtually all the fluid within the lens. Furthermore, because radial gradients are expected to be reduced within the boundary layer, the boundary layer effect can be approximated by simply using a reduced effective lens length. Gradients in the  $z$  direction are expected to be much larger within the boundary layer because the fluid velocity transitions to zero at the wall. However, for a normally incident beam of light, all that is significant is the transverse gradient in total optical path length through the lens. Optical path length differences due to density gradients in the  $z$  direction within the thin boundary layer are insignificant compared to the optical path length differences within the bulk. The result of these considerations is that an approximate solution can be found by solving the one dimensional problem, assuming  $\rho$  is only a function of  $r$  and then applying that solution to all values of  $z$  within the lens.

The problem can be further simplified by linearization. This assumes that the acoustic waves have a small amplitude relative to static conditions. We expand each variable in terms of an arbitrary amplitude parameter,  $\lambda$

$$\rho(r, t) = \rho_0 + \lambda\rho_1(r, t) + \lambda^2\rho_2(r, t) + \dots, \quad (9)$$

$$\mathbf{v}(r, t) = 0 + \lambda\mathbf{v}_1(r, t) + \lambda^2\mathbf{v}_2(r, t) + \dots. \quad (10)$$

Furthermore, we assume that the wave amplitudes are small and therefore that any second order or higher term ( $\lambda^2$ ,  $\lambda^3$ , etc.) is much less than the zeroth or first order terms, and that the higher order terms can be dropped from the equations. Keeping only the zeroth and first order terms results in  $\rho(r, t) = \rho_0 + \lambda\rho_1(r, t)$  and  $\mathbf{v}(r, t) = \lambda\mathbf{v}_1(r, t)$ ; and Eqs. (2) and (3) can be rewritten as

$$\lambda\left[\frac{\partial\rho_1}{\partial t} + \nabla \cdot (\rho_0\mathbf{v}_1)\right] = 0, \quad (11)$$

$$\lambda\left[\frac{\partial}{\partial t}(\rho_0\mathbf{v}_1) + c_s^2\nabla\rho_1 + \nabla \cdot \mathbf{D}_1\right] = 0, \quad (12)$$

where  $\mathbf{D}_1$  is defined in the same way as  $\mathbf{D}$  in Eq. (5), except with  $\mathbf{v}$  replaced by  $\mathbf{v}_1$ .

### 1. Inviscid solution

One solution of interest is the inviscid solution because it reasonably accurately predicts the lens output patterns for low viscosities in off-resonant conditions while retaining a simple analytic form. This solution is found by setting  $\mu = \eta = 0$ . In the one dimensional case, the problem becomes

$$\frac{\partial\rho_1}{\partial t} + \frac{1}{r}\frac{\partial}{\partial r}(r\rho_0v) = 0, \quad (13)$$

$$\frac{\partial}{\partial t}(\rho_0v) + c_s^2\frac{\partial\rho_1}{\partial r} = 0, \quad (14)$$

$$v|_{r=r_0} = v_A \cos(\omega t). \quad (15)$$

It can be directly verified by substitution that the solution to this problem is

$$\rho_1(r, t) = \rho_A J_0(\omega r/c_s) \sin(\omega t), \quad (16)$$

$$v(r, t) = -\frac{\rho_A c_s}{\rho_0} J_1(\omega r/c_s) \cos(\omega t), \quad (17)$$

where  $\rho_A = -(\rho_0 v_A)/[c_s J_1(\omega r_0/c_s)]$ . For the base case off-resonant frequency,  $\rho_A$  is expected to be  $0.090 \text{ kg/m}^3$ .

## 2. Viscous solution

We start by defining an effective kinematic viscosity,  $\nu' \equiv (\eta + 4\mu/3)$ . In cases where this viscosity is large compared to  $c_s^2/\omega$  or when the lens is driven near a resonant frequency of the cavity, viscosity becomes significant and the solution is somewhat more complex. To put the viscosity threshold in context, the base case fluid, 100 cS silicone oil, is considered low viscosity for frequencies  $f \ll c_s^2/(2\pi\nu') = 700 \text{ MHz}$ .

We start by differentiating Eq. (11) with respect to time, and taking the divergence of Eq. (12) so that the equations can be decoupled and all dependence on  $\mathbf{v}$  eliminated to yield the damped wave equation

$$\nabla^2 \left( c_s^2 \rho_1 + \nu' \frac{\partial \rho_1}{\partial t} \right) - \frac{\partial^2 \rho_1}{\partial t^2} = 0. \quad (18)$$

By evaluating Eqs. (11) and (12) at  $r=r_0$  and assuming a curl-free velocity field there, Eq. (6) can be converted from a boundary condition in velocity to the following Neumann boundary condition in density

$$\left. \frac{\partial \rho_1}{\partial r} \right|_{r=r_0} = \frac{\rho_0 v_A \omega c_s^2}{\nu'^2 \omega^2 + c_s^4} \sin(\omega t) - \frac{\rho_0 v_A \omega^2 \nu'}{\nu'^2 \omega^2 + c_s^4} \cos(\omega t). \quad (19)$$

The steady-state one-dimensional solution to the above wave equation and boundary condition can be expanded as a sum of eigenfunctions

$$\rho_1(r, t) = r(A \sin(\omega t) + B \cos(\omega t)) + \sum_{m=0}^{\infty} J_0(k_m r) \times [C_m \sin(\omega t) + D_m \cos(\omega t)], \quad (20)$$

where  $k_m = x_m/r_0$  with  $x_m$  being the location of the  $m$ th zero of  $J_1(x)$  and  $x_0=0$ .  $A$  and  $B$  can be found by substituting this solution into Eq. (19).  $C_m$  and  $D_m$  can be found by substituting the solution into Eq. (18) and integrating against the orthogonal eigenfunction  $J_0(k_m r)$  over the entire circular domain. The resulting expressions are

$$A = \frac{\rho_0 v_A \omega c_s^2}{\nu'^2 \omega^2 + c_s^4}, \quad (21)$$

$$B = -\frac{\rho_0 v_A \omega^2 \nu'}{\nu'^2 \omega^2 + c_s^4}, \quad (22)$$

$$C_m = \left( \frac{2\rho_0 v_A \omega}{J_0^2(k_m r_0)} \right)$$

$$\times \frac{E_m r_0 \omega^2 \frac{k_m^2 (c_s^4 - \omega^2 \nu'^2) - c_s^2 \omega^2}{\nu'^2 \omega^2 + c_s^4} - \frac{F_m}{r_0} (\omega^2 - c_s^2 k_m^2)}{\omega^2 (\omega^2 - 2c_s^2 k_m^2) + k_m^4 (\nu'^2 \omega^2 + c_s^4)}, \quad (23)$$

$$D_m = \left( \frac{2\rho_0 v_A \omega}{J_0^2(k_m r_0)} \right) \omega \nu' \frac{E_m r_0 \omega^2 \frac{\omega^2 - 2c_s^2 k_m^2}{\nu'^2 \omega^2 + c_s^4} - \frac{F_m k_m^2}{r_0}}{\omega^2 (\omega^2 - 2c_s^2 k_m^2) + k_m^4 (\nu'^2 \omega^2 + c_s^4)}. \quad (24)$$

In the expressions above,  $E_m$  and  $F_m$  are the nondimensional integrals

$$E_m = \int_0^1 x^2 J_0(x_m x) dx, \quad (25)$$

$$F_m = \int_0^1 J_0(x_m x) dx. \quad (26)$$

By taking the limit  $\nu' \rightarrow 0$  and using the same trick of integrating against an orthogonal eigenfunction, the inviscid solution in Eq. (16) can be recovered.

## 3. Resonant driving conditions

Another important limit is that of operating near a resonance of the cavity using a relatively low viscosity fluid. Operating at the  $n$ th ( $>0$ ) resonance means that  $\omega = c_s k_n$ . Note that at resonant frequencies, the inviscid solution in Eq. (16) diverges because  $J_1(kr_0) \rightarrow 0$  in the denominator of  $\rho_A$ . Consequently, in order to get a valid solution near resonance, the full viscous solution is necessary, even at low viscosities. As discussed in the previous section, low viscosity means that  $\nu' \ll c_s^2/\omega$ . In this limit, the coefficients of the viscous solution look as follows:

$$A \rightarrow \frac{\rho_0 v_A k_n}{c_s}, \quad (27)$$

$$B \rightarrow -\nu' \frac{k_n}{c_s} \left( \frac{\rho_0 v_A k_n}{c_s} \right), \quad (28)$$

$$C_{m \neq n} \rightarrow \left( \frac{2\rho_0 v_A \omega}{J_0^2(k_m r_0)} \right) \frac{E_m r_0 k_n^2 + \frac{F_m}{r_0}}{c_s^2 (k_m^2 - k_n^2)}, \quad (29)$$

$$C_{m=n} \rightarrow -\left( \frac{2\rho_0 v_A \omega}{J_0^2(\omega r_0/c_s)} \right) \frac{E_n r_0}{c_s^2}, \quad (30)$$

$$D_{m \neq n} \rightarrow -\nu' \left( \frac{2\rho_0 v_A \omega}{J_0^2(k_m r_0)} \right) \frac{\omega}{c_s^2} \frac{E_m r_0 k_n^2 (k_m^2 - k_n^2) + \frac{F_m k_m^2}{r_0}}{c_s^2 (k_m^2 - k_n^2)^2}, \quad (31)$$

$$D_{m=n} \rightarrow -\frac{1}{\nu'} \left( \frac{2\rho_0 v_A \omega}{J_0^2(\omega r_0/c_s)} \right) \frac{c_s^2 (E_n r_0 k_n^2 + F_n r_0)}{\omega^3}. \quad (32)$$

Note that as the viscosity vanishes, the only term that diverges is the  $D_{m=n}$  term. All the other terms either vanish or do not change. This means that when driving on resonance with a low viscosity fluid only the  $D_{m=n}$  term is significant, and the solution for the density becomes

$$\rho_1(r,t) \rightarrow -\frac{1}{\nu'} \left( \frac{2\rho_0 v_A c_s^2 \left( E_n r_0 \frac{\omega^2}{c_s^2} + \frac{F_n}{r_0} \right)}{\omega^2 J_0^2(\omega r_0/c_s)} \right) J_0 \left( \frac{\omega r}{c_s} \right) \times \cos(\omega t). \quad (33)$$

At the resonant base case frequency, the amplitude of  $\rho_1$  takes the value  $9.1 \text{ kg/m}^3$ .

### C. From density to refractive index

The Lorentz–Lorenz equation<sup>30</sup> can be used to determine the local index of refraction from the fluid density. This relationship is

$$n = \sqrt{\frac{2Q\rho + 1}{1 - Q\rho}}, \quad (34)$$

where  $Q$  is the molar refractivity, which can be determined from  $n_0$  and  $\rho_0$ . For small  $\rho_1$ , this equation can be linearized by a Taylor expansion about the static density and refractive index. Substituting for  $Q$ , this takes the form

$$n = n_0 + \frac{n_0^4 + n_0^2 - 2}{6n_0} \left( \frac{\rho_1}{\rho_0} \right). \quad (35)$$

In the resonant base case, the amplitude of oscillation of the density standing wave is less than 1% of the static density. Comparing the true Lorentz–Lorenz equation with the linearized version, one finds that the error in refractive index due to linearization is less than 0.2%.

In the inviscid linearized acoustic case, the refractive index given by Eq. (35) assuming the density distribution in Eqs. (16) or (33), depending on resonance, reduces to an expression of the form

$$n = n_0 + n_A J_0(kr) \sin(\omega t), \quad (36)$$

in the off-resonant case, or

$$n = n_0 + n_A J_0(kr) \cos(\omega t), \quad (37)$$

at resonance. The full expression for  $n_A$  in the low-viscosity off-resonant case is

$$n_A = \left( \frac{n_0^4 + n_0^2 - 2}{6n_0} \right) \left( \frac{-v_A}{c_s J_1(\omega r_0/c_s)} \right), \quad (38)$$

and in the resonant case,  $n_A$  is given by

$$n_A = \left( \frac{n_0^4 + n_0^2 - 2}{6n_0} \right) \left( \frac{-2c_s^2 v_A}{\nu' \omega^2 J_0^2(\omega r_0/c_s)} \right) \left( E_n r_0 \frac{\omega^2}{c_s^2} + \frac{F_n}{r_0} \right). \quad (39)$$

For the base case,  $n_A$  is expected to have an off-resonant value of  $4.3 \times 10^{-5}$ . On resonance, it is expected to have a

base case value of  $4.3 \times 10^{-3}$ . Similar solutions can be obtained for the viscous case.

## IV. OPTIMIZING THE FIGURE OF MERIT: REFRACTIVE POWER

In order to get the most out of a TAG lens under steady state operation, one wishes to maximize the peak refractive power. The lower bound is always zero, given by the static lens without any input driving signal. Higher refractive powers increase the range of achievable working distances and Bessel beam ring spacing. The refractive power,  $RP$ , is defined here to be the magnitude of the transverse gradient in optical path length. This is given by the product of the transverse gradient in refractive index and the length of the lens. Under thin lens and small angle approximations, the maximum angle that an incoming collimated ray can be diverted by the TAG lens is equal to its refractive power.<sup>31</sup> For a simple converging lens, its  $RP$  is also equal to its numerical aperture.

Maximizing the refractive power can be accomplished by altering the dimensions of the lens, the filling fluid, or the driving signal. Because the base case TAG lens is well within the low viscosity range of the parameter space, discussion in this section will be limited to only low-viscosity fluids in the resonant and off-resonant cases so that Eq. (36) or (37) applies with  $n_A$  given by Eq. (38) or (39).

The first step is to calculate the TAG lens peak refractive power,  $RP_A$ , using Eq. (36) and assuming azimuthal symmetry within the lens

$$\begin{aligned} RP_A &\equiv \max_{r>0} |\nabla \text{OPL} \cdot \hat{\mathbf{r}}| \\ &= \max_{r>0} |L \nabla n \cdot \hat{\mathbf{r}}| \\ &= \max_{r>0} |L k n_A J_1(kr)|. \end{aligned} \quad (40)$$

Therefore,  $RP_A$  is maximized by maximizing  $|L k n_A|$ , while the term  $J_1(kr)$  only determines at what radial location this maximum is achieved. In order to maximize  $|L k n_A|$ , we look at each of the parameters in Eqs. (38) and (39). Because the dependence on these parameters can vary between resonant and off-resonant driving conditions, the analysis has been divided into the two sections below.

### A. Optimizing resonant conditions

First we assume that the lens will be driven under resonant conditions. This will yield the highest refractive powers. At the resonant base case frequency,  $RP_A$  takes the value 0.16. The model for this section uses the refractive index given by Eq. (37) with  $n_A$  given by Eq. (39).

#### 1. Optimizing lens dimensions

First we consider the size of the TAG lens. This is determined by the piezoelectric length  $L$  and inner radius  $r_0$ . The refractive power of the TAG lens is proportional to  $L$ , so longer lenses are desirable. With increasing length, thin lens

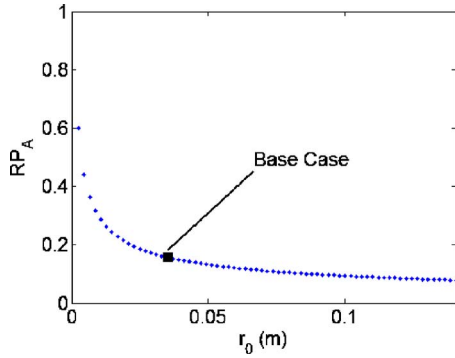


FIG. 3. (Color online) Dependence of the peak refractive power of the lens,  $RP_A$ , on the inner radius of the lens,  $r_0$ , assuming resonant driving conditions.

approximations will become increasingly erroneous, and eventually the TAG lens will function as a waveguide.

The dependence on transverse lens size is not a simple relationship because of the Bessel functions in the denominator of Eq. (39) and the fact that the value of  $n$  in  $E_n$  and  $F_n$  depends on  $r_0$ . The relationship between the refractive power and the inner lens radius is plotted in Fig. 3. This figure shows that on resonance, higher refractive powers can be achieved with lenses having a smaller radius. Discrete points are plotted because resonance is only achieved at discrete inner radii. This effect can be attributed to increased viscous losses due to increased acoustic wave propagation distance.

**2. Optimizing the refractive fluid**

The relevant properties of the refractive fluid include its static index of refraction  $n_0$ , its effective kinematic viscosity  $\nu'$ , and the speed of sound within the material,  $c_s$ .

Increasing the value of  $n_0$  affects only the first term of Eq. (39) and increases the TAG lens refractive power. Due to the nature of the Lorentz–Lorenz equation, the same fractional variation in density will have a greater effect on the refractive index of a material with a naturally high refractive index than it will on a material with a lower refractive index. This effect is plotted in Fig. 4. It is clear that higher static indices of refraction improve lens performance.

In the resonant case, the viscosity of the fluid is significant and lower viscosities are more desirable because the refractive index amplitude is inversely proportional to the

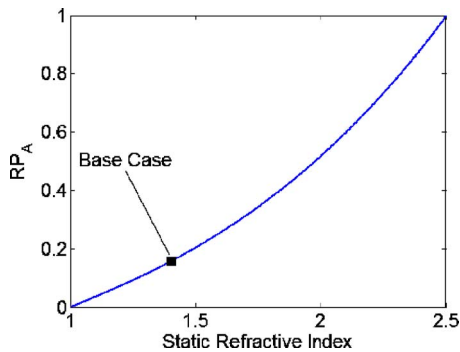


FIG. 4. (Color online) Dependence of the peak refractive power of the lens,  $RP_A$ , on the static refractive index,  $n_0$ , assuming resonant driving conditions.

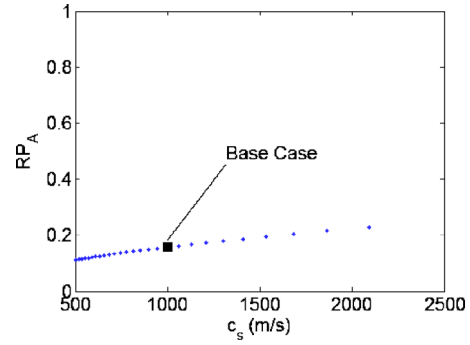


FIG. 5. (Color online) Dependence of the peak refractive power,  $RP_A$ , on fluid sound speed,  $c_s$ , assuming resonant driving conditions.

effective kinematic viscosity. In symbols,  $n_A \propto \nu'^{-1}$ . This result is expected because lower viscosities will mean less viscous loss of energy within the lens.

As with the inner radius, the effect of the sound speed on the refractive power cannot be easily analytically represented because of the Bessel functions in the denominator of Eq. (39) and the dependence of  $E_n$  and  $F_n$  on  $c_s$ . These effects are plotted in Fig. 5. This shows that higher sound speeds are preferable.

Listed in Table II are variety of filling materials and their relevant properties. For resonant driving conditions, water and 0.65 cS silicone oil are best because of their low viscosities. Nitrogen would make a poor choice because of its very low value of static index of refraction. Because of their high viscosities, Glycerol and 100 cS silicone oil are less desirable for resonant operation.

**3. Optimizing the driving signal**

This article only covers sinusoidal driving signals; however, more complicated signals can be used to produce arbitrary index profiles that repeat periodically in time.<sup>32</sup> There are two variable parameters of the sinusoidal driving signal: Its amplitude,  $V_A$ , and its frequency,  $\omega$ . These two parameters will determine the inner wall velocity,<sup>25</sup> which this paper treats as a given parameter.

It has been noted that voltage amplitude,  $V_A$ , is proportional to inner wall velocity,  $v_A$ . These amplitudes have a very simple effect on the refractive index. From Eqs. (38) and (39), it can be seen that lens refractive power is directly proportional to  $v_A$ , and hence,  $V_A$ , and that larger wall velocities and driving voltages are desirable.

Similar to the lens radius and sound speed, the driving frequency  $\omega$  has an effect on the refractive power of the lens

TABLE II. Properties of potential filling fluids. All values are for temperatures in the 20 °C–30 °C range.

| Fluid        | $n_0$  | $\nu$ (cS) | $c_s$ (m/s) | $\rho_0$ (kg/m <sup>3</sup> ) |
|--------------|--------|------------|-------------|-------------------------------|
| Silicone oil | 1.4030 | 100        | 985         | 964                           |
| Silicone oil | 1.375  | 0.65       | 873.2       | 761                           |
| Glycerol     | 1.4746 | 740        | 1904        | 1260                          |
| Water        | 1.33   | 1.00       | 1493        | 1000                          |
| Nitrogen     | 1.0003 | 16.1       | 355         | 1.12                          |

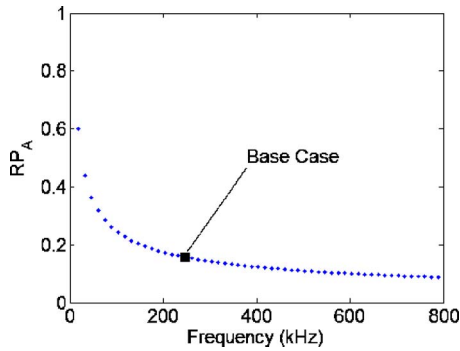


FIG. 6. (Color online) Dependence of refractive power on driving frequency  $f = \omega / (2\pi)$ , assuming resonant driving conditions.

that cannot be given in a simple analytic form. This effect is plotted in Fig. 6 and illustrates that lower frequencies yield greater refractive powers. This is because higher frequencies exhibit greater viscous damping.

### B. Optimizing nonresonant conditions

There are conditions where driving on resonance is impractical. For example, due to the sharpness of the resonant peaks, a small error in lens properties or driving frequency can result in a large error in refractive index. Operating off resonance can be more forgiving in terms of error, however, this comes at the expense of reduced refractive powers. In this section we use the off-resonant base case frequency. Since the lens is operating off resonance, the refractive index is given by Eq. (36) with  $n_A$  given by Eq. (38), which yields an  $RP_A$  of 0.0016.

The dependencies of  $RP_A$  on lens length  $L$ , static refractive index  $n_0$ , and driving amplitude  $V_A$  ( $v_A$ ) are all identical to what was found for resonant driving conditions. This is because these variables only appear in the common prefactors in Eqs. (38) and (39). Hence these parameters will not be reexamined in this section. Note that if referring to Fig. 4 ( $RP_A$  vs  $n_0$ ), the  $RP$  axis will have to be scaled appropriately because the values of  $RP_A$  differ between the resonant and off-resonant cases.

The difference between the resonant and off-resonant driving conditions is found in the lens radius  $r_0$ , the sound speed  $c_s$ , and the driving frequency  $\omega$ . These dependencies are plotted in Figs. 7–9. These parameters all exhibit oppo-

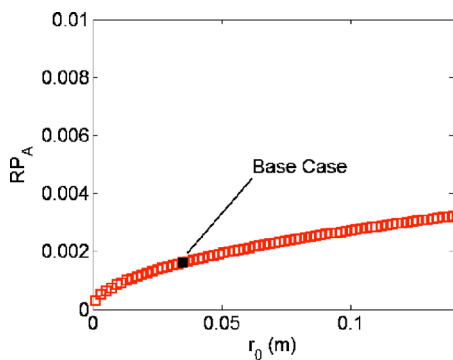


FIG. 7. (Color online) Nonresonant dependence of the refractive power of the lens,  $RP_A$ , on the inner radius of the lens,  $r_0$ .

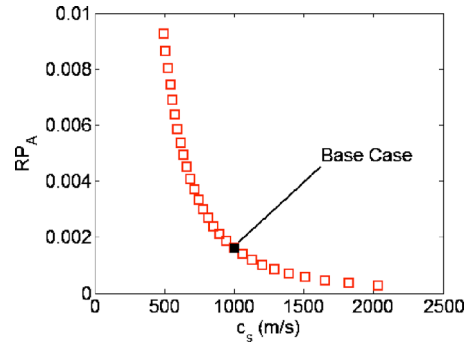


FIG. 8. (Color online) Nonresonant dependence of refractive power,  $RP_A$ , on fluid sound speed,  $c_s$ .

site trends from resonant driving conditions. For best off-resonant performance, large radius lenses filled with low speed of sound fluids driven at high frequencies are desirable. This occurs because viscous damping no longer affects the refractive power. We expect these results because larger lenses vibrating at the same wall speed cause more acoustic power to be focused at the center of the lens, increasing refractive powers. Also, higher driving frequencies condenses the spatial oscillations in density, producing higher gradients in refractive index.

Looking at the values in Table II, it is evident that for off-resonant driving, both silicone oils, glycerol, and water all become viable fluid choices now that viscosity is unimportant. These fluids all have appreciable static refractive indices compared to nitrogen. The silicone oils are expected to have somewhat better performance over glycerol and water because of their low sound speeds.

### C. Other considerations

Preventing cavitation is another consideration involved in selecting a filling material other than simply maximizing the refractive power. If the pressure within the lens drops below the vapor pressure of the fluid, then cavitation can occur, producing bubbles within the lens that disrupt its optical capability. Specifically, this can happen when

$$p_A > p_0 - p_v / c_s^2, \quad (41)$$

where  $p_v$  is the vapor pressure of the fluid. There are a couple ways that cavitation can be avoided. First, one can

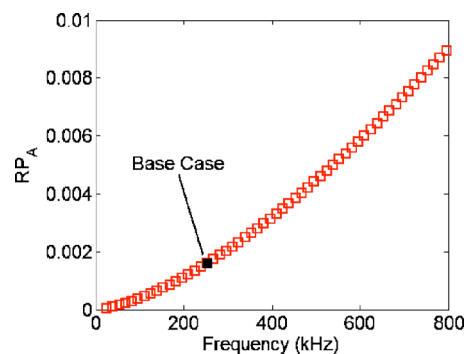


FIG. 9. (Color online) Nonresonant dependence of refractive power on driving frequency  $f = \omega / (2\pi)$ .

choose a fluid with a low vapor pressure. Second, the lens can be filled to a high static pressure.

Another danger in blindly maximizing the refractive power is that at high  $RP$  values, the model may break down. This is because the linearization performed in Sec. III B is only valid at relatively small amplitudes. Once the order of  $\rho_A$  or  $n_A$  becomes comparable to the order of  $\rho_0$  or  $n_0$ , the linearization loses accuracy. It is likely that the general trends observed in this section will hold to some degree in the nonlinear regime, although the specific form of the dependence of refractive power on all the variables requires further analysis. It is possible to increase the domain of the linear regime by selecting fluids of large density. One should also note that the selection of  $n_0$  does not affect the linearization of the fluid mechanics. Therefore, increasing the refractive power via increasing the fluid's refractive index will not endanger the fluid linearization, although it may endanger the Lorentz–Lorenz linearization. However, when the linear models no longer apply, it is still possible to obtain solutions via full numerical simulations.

## V. TUNABILITY

What makes the TAG lens particularly attractive for beam shaping applications is its ability to tune the multiscale Bessel beam ring spacing and extent via driving voltage frequency and amplitude.<sup>22</sup> This potential is best seen by considering Eqs. (36) and (37).

As discussed above, both voltage amplitude and frequency affect the amplitude  $n_A$  of the refractive index standing wave. Adjusting the value of  $n_A$  can be used to tune the minor ring interference patterns surrounding the major rings in Fig. 1. This is analogous to changing the cone angle of a fixed axicon. Adjusting  $n_A$  will not affect the location of the major rings.

The location of the major rings is determined by the driving frequency and is independent of the driving voltage amplitude. The locations of the major rings occur at the extrema of the function  $J_0(\omega r/c_s)$ . Increasing the driving frequency will condense the major rings and decreasing the driving frequency will expand the major rings. For example, the radial coordinate of the first major ring,  $r^*$  is given by

$$r^* = \frac{3.832c_s}{\omega}, \quad (42)$$

where 3.832 is the radial coordinate of the first minimum of  $J_0(r)$ .

## VI. CONCLUSIONS

This article has provided the first step toward fine control of tunable acoustic gradient index lenses: A predictive model of the dynamics of the lens. The results are useful for optimizing the TAG lens design in terms of maximizing its ability to refract light in steady-state operation. A TAG lens is most effective when it is long, filled with a fluid of high refractive index, and driven with large voltage amplitudes. If driving on resonance, lower frequencies, smaller lens radii, and fluids with larger sound speeds and lower viscosities

enhance refractive power. Off resonance, higher frequencies, larger lenses, and lower sound speeds are preferred. Viscosity is irrelevant for nonresonant driving.

It is important to note that these choices are only best for optimizing the steady-state refractive power where the linear model of Sec. III is applicable. If wave amplitudes become too great, then a nonlinear model will be required, which could be implemented numerically. Also, different optimization parameters will occur if, for example, one wishes to optimize the TAG lens for pattern switching speed or high damage thresholds—two of the potential advantages of TAG lenses over spatial light modulators.

The above modeling has been done in a circular geometry so as to model a TAG lens capable of generating Bessel beams. Other geometries are also possible for creating complicated beam patterns. The natural example is that of a rectangular cavity in which the Bessel eigenfunctions would be replaced by sines and cosines. With other geometries that break the circular symmetry, it may also be possible to create Laguerre–Gaussian and higher-order Bessel beams. It has been shown that passing a Laguerre–Gaussian beam through an axicon creates higher-order Bessel beams.<sup>33</sup> This same method can be implemented with the TAG lens replacing the axicon to produce tunable higher order Bessel modes.

In the linear regime, this cylindrical TAG lens also has the potential to create arbitrary (non-Bessel) radially-symmetric beams. By driving the lens with a Fourier series of signals at different frequencies, interesting refractive index distributions within the lens can be generated. This is because the lens effectively performs a Fourier–Bessel transform of the electrical signal into the index pattern. As this pattern will vary periodically in both space and time, it will be best resolved with a pulsed laser synchronized to the TAG lens.

## ACKNOWLEDGMENTS

We wish to thank Adam B. Hopkins for initial investigations into the physics of the TAG lens and Ed Rietman for introducing us to acoustic lenses. Mikko Haataja, Jason Fleischer, and Clancy Rowley have provided useful discussions. Princeton University and USAFOSR have provided financial support.

<sup>1</sup>J. Durnin, J. Opt. Soc. Am. A **4**, 651 (1987).

<sup>2</sup>J. Durnin and J. J. J. Miceli, Phys. Rev. Lett. **58**, 1499 (1987).

<sup>3</sup>Y. Lin, W. Seka, J. H. Eberly, H. Huang, and D. L. Brown, Appl. Opt. **31**, 2708 (1992).

<sup>4</sup>G. Indebetouw, J. Opt. Soc. Am. A **6**, 150 (1989).

<sup>5</sup>D. McGloin and K. Dholakia, Contemp. Phys. **46**, 15 (2005).

<sup>6</sup>J. Turunen, A. Vasara, and A. T. Friberg, Appl. Opt. **27**, 3959 (1988).

<sup>7</sup>J. Amako, K. Yoshimura, D. Sawaki, and T. Shimoda, in *Laser-Based Microprocesses Using Diffraction-Free Beams Generated by Diffractive Axicons*, in *Photon Processing in Microelectronics and Photonics IV*, Proceedings of SPIE, Vol. 5713, edited by J. Fieret *et al.* (SPIE, Bellingham, WA, 2005), pp. 497–507.

<sup>8</sup>Y. Matsuoka, Y. Kizuka, and T. Inoue, Appl. Phys. A: Mater. Sci. Process. **84**, 423 (2006).

<sup>9</sup>J. Amako, D. Sawaki, and E. Fujii, J. Opt. Soc. Am. B **20**, 2562 (2003).

<sup>10</sup>E. Gaizauskas and E. Vanagas, Opt. Lett. **31**, 80 (2006).

<sup>11</sup>J. A. Davis, J. Guertin, and D. M. Cottrell, Appl. Opt. **32**, 6368 (1993).

<sup>12</sup>J. A. Davis, E. Carcole, and D. M. Cottrell, Appl. Opt. **35**, 599 (1996).

<sup>13</sup>N. Chattaripban, E. A. Rogers, D. Cofield, I. Wendell, T. Hill, and R. Roy, Opt. Lett. **28**, 2183 (2003).

- <sup>14</sup>J. Leach, G. M. Gibson, and M. J. Padgett, *Opt. Express* **14**, 5581 (2006).
- <sup>15</sup>V. Garcés-Chavez, D. McGloin, H. Melville, W. Sibbett, and K. Dholakia, *Nature* **419**, 145 (2002).
- <sup>16</sup>T. Čižmár, V. Garcés-Chávez, K. Dholakia, and P. Zemánek, *Appl. Phys. Lett.* **86**, 174101 (2005).
- <sup>17</sup>M. D. Summers, J. P. Reid, and D. McGloin, *Opt. Express* **14**, 6373 (2006).
- <sup>18</sup>K. Okamoto, Y. Inouye, and S. Kawata, *Jpn. J. Appl. Phys., Part 1* **40**, 4544 (2001).
- <sup>19</sup>E. H. Trepagnier *et al.*, *Proc. Natl. Acad. Sci. U.S.A.* **101**, 15038 (2004).
- <sup>20</sup>G. M. Wang, E. M. Sevick, E. Mittag, D. J. Searles, and D. J. Evans, *Phys. Rev. Lett.* **89**, 050601 (2002).
- <sup>21</sup>D. McGloin, V. Garcés-Chavez, and K. Dholakia, *Opt. Lett.* **28**, 657 (2003).
- <sup>22</sup>E. McLeod, A. B. Hopkins, and C. B. Arnold, *Opt. Lett.* **31**, 3155 (2006).
- <sup>23</sup>T. Tsai, E. McLeod, and C. B. Arnold, in *Generating Bessel Beams with a Tunable Acoustic Gradient Index of Refraction Lens*, in Proceedings of SPIE, Vol. No. 6326, edited by K. Dholakia and G. C. Spalding (SPIE, Bellingham, WA, 2006), p. 63261F.
- <sup>24</sup>K. A. Higginson, M. A. Costolo, and E. A. Rietman, *Appl. Phys. Lett.* **84**, 843 (2004).
- <sup>25</sup>N. T. Adelman, Y. Stavsky, and E. Segal, *J. Sound Vib.* **38**, 245 (1975).
- <sup>26</sup>H. Metiu and K. F. Freed, *J. Chem. Phys.* **67**, 3303 (1999).
- <sup>27</sup>R. E. Graves and B. M. Argrow, *J. Thermophys. Heat Transfer* **13**, 337 (1999).
- <sup>28</sup>J. Xu, X. Ren, W. Gong, R. Dai, and D. Liu, *Appl. Opt.* **42**, 6704 (2003).
- <sup>29</sup>P. M. Morse and K. U. Ingard, *Theoretical Acoustics* (McGraw-Hill Book Company, New York, 1968).
- <sup>30</sup>M. Born and E. Wolf, *Principles of Optics* (Cambridge University Press, Cambridge, 2003).
- <sup>31</sup>E. McLeod and C. B. Arnold (unpublished).
- <sup>32</sup>E. McLeod and C. B. Arnold, *Complex Beam Sculpting with Tunable Acoustic Gradient Index Lenses*, in Proceedings of SPIE, Vol. No. 6483, edited by D. L. Andrews, E. J. Galvez, and G. Nienhuis (SPIE, Bellingham, WA, 2007), p. 64830I.
- <sup>33</sup>J. Arlt and K. Dholakia, *Opt. Commun.* **177**, 297 (2000).